CrossMark
click for updates

Empirical determination of the energy band gap narrowing in highly doped n$^+$ silicon

Di Yan[a)] and Andres Cuevas
Research School of Engineering, The Australian National University, Canberra, ACT 0200, Australia

Highly doped regions in silicon devices should be analyzed using Fermi-Dirac statistics, taking into account energy band gap narrowing (BGN). An empirical expression for the BGN as a function of dopant concentration is derived here by matching the modeled and measured thermal recombination current densities J_0 of a broad range of n$^+$ dopant concentration profiles prepared by phosphorus diffusion. The analysis is repeated with Boltzmann statistics in order to determine a second empirical expression for the *apparent* energy band gap narrowing, which is found to be in good agreement with previous work. © 2013 AIP Publishing LLC.
[http://dx.doi.org/10.1063/1.4816694]

I. INTRODUCTION

In most silicon solar cells and other electronic devices, highly doped n$^+$ and p$^+$ regions are usually formed near the surfaces to suppress the concentration of one type of charge carrier and facilitate the selective transport of the other type towards an external circuit. For example, a highly doped n$^+$ region offers a high conductivity for electrons and, in principle, results in a small concentration of holes, both in equilibrium and under weak excitation. This is, however, compromised by energy band gap narrowing effects (BGN),[1,2] which tend to increase the equilibrium minority carrier concentration. The consequence of BGN combined with Auger and surface recombination is that n$^+$ and p$^+$ regions frequently limit the performance of silicon solar cells.

Since the concentrations of minority and majority carriers are coupled, determining the latter is also necessary. The number of available quantum states in the majority carrier band is commonly simplified to an effective density of states ($N_c = 2.86 \times 10^{19}$ cm^{-3} and $N_v = 3.1 \times 10^{19}$ cm^{-3} *at* 300 K),[3] which multiplied by a Boltzmann-type exponential factor gives the concentration of majority carriers in moderately doped Si. When the carrier concentration approaches N$_c$ or N$_v$, as occurs in highly doped n$^+$ and p$^+$ Si, the semiconductor becomes degenerate (i.e., more carriers than effective states) and an analysis using Fermi-Dirac statistics becomes necessary. Although degeneracy is a well-known fact, it has been common practice for many years to lump together the effects of energy band gag narrowing (BGN) and degeneracy (FD statistics) into a mathematically convenient parameter that has been called the *apparent* BGN. Such terminology has also taken root in the experimental realm, due to the fact that most measurements of the energy band gap narrowing have been analyzed using Boltzmann statistics. This means that to replicate the original measurements, Boltzmann statistics should be used when modeling heavily doped regions if an empirical parameterization of the *apparent* BGN as a function of dopant density[4] is used. This is the approach followed by the popular simulation program PC1D.[5] On the other hand, Sentaurus TCAD[6] and EDNA[7] give the option to use Fermi-Dirac statistics in conjunction with the BGN model developed by Schenk.[8] Although this second approach is more rigorous, it relies on a theoretical BGN model, and needs to be tested experimentally.

The test performed here is based on a large set of phosphorus diffused regions and measurements of the corresponding recombination current pre-factors J$_0$ and dopant density profiles. As shown in Sec. III, the J_0 simulated with Fermi-Dirac statistics and Schenk's BGN[8] is inconsistent with the measured J_0. This means that the model for the BGN needs to be revised. We do that in Sec. IV using those same experimental measurements to extract the BGN as a function of dopant density, following a similar approach to that of Refs. 4, 9, and 10, but using Fermi-Dirac statistics. In addition, we repeat the analysis of minority carrier transport in the n$^+$ regions using Boltzmann statistics, in order to give an empirical expression for the *apparent* BGN. Although sound physics demands that Fermi-Dirac statistics should be used, either approach is consistent with our experiment, provided that the appropriate empirical expression for either the BGN or the *apparent* BGN is used.

II. EXPERIMENTAL METHODS

A range of dopant density profiles was created by phosphorus diffusion and oxidation/drive-in steps on $100\,\Omega$ cm p-type wafers (N$_A$ = 1.3×10^{14} cm^{-3}) with a thickness of $500 \pm 10\,\mu$m. The phosphorus pre-depositions were performed within a temperature range of 760–840 °C using POCl$_3$ as a dopant source. The drive-in step was carried out in pure oxygen within the temperature range of 900–1000 °C for 30–60 min, after having removed the phosphorus-silica glass. A total of 24 different dopant profiles were generated, with sheet resistances between $11.5 \pm 0.5\,\Omega/\square$ and $292.5 \pm 24\,\Omega/\square$, and surface dopant concentrations from $(3.67 \pm 0.29) \times 10^{18}$ cm^{-3} to $(1.15 \pm 0.07) \times 10^{20}$ cm^{-3}. The corresponding dopant density profiles were measured using an electrochemical capacitance-voltage instrument (WEP Wafer Profiler CVP21), some of them are shown in Fig. 1. It is worth noting that ECV measurements give the concentration of
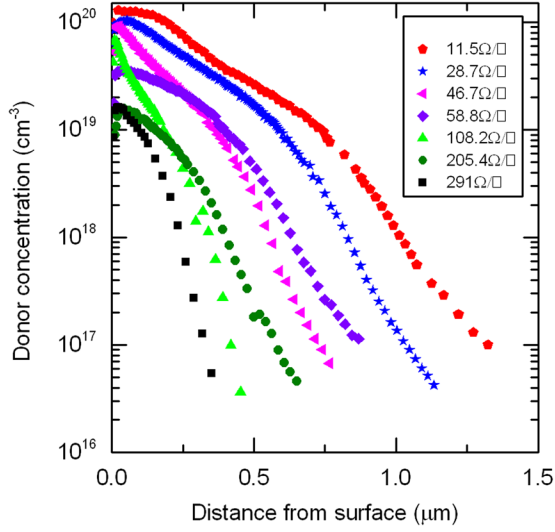
a)Electronic mail: di.yan@anu.edu.au

FIG. 1. Electrically active phosphorus concentration profiles of several silicon samples with different sheet resistances.

FIG. 2. Measured J_0 of different phosphorus diffusions as a function of the surface dopant concentration. The corresponding sheet resistances are shown as a color scale.

electrically active dopants, that is, the concentration of majority carriers, in this case electrons. Due to the fact that inconstant contact area results in an underestimation when calculating the doping concentration in the ECV measurement, the absolute value of the dopant concentration was determined by matching the sheet resistance calculated for every dopant profile to that measured by two additional methods, a four point probe (Signatone, model S-301-4) and a calibrated inductive-coil conductance tester from Sinton Instruments.[11] The latter measures the sheet resistance averaged over a 3 cm^2 area, precisely the same, and at the same location, where the recombination current density J_0 was measured using the same instrument. The ECV measurements therefore represent the dopant profiles averaged over the area relevant to the measurement of J_0.

After all silicon oxides are removed from the surface in a dilute HF solution, semi-transparent aluminum layers with thicknesses between 10 *and* 20 nm were deposited symmetrically on the two phosphorus diffused sides of each wafer to ensure that the velocity of carriers at the surface is approximately equal to its kinetic limit. The recombination current pre-factor J_0 of each sample was then measured at room temperature following the method proposed by Kane and Swanson[12] by both photo-conductance decay (PCD)[12] and Quasi-Steady-State photo-conductance (QSSPC)[13] at an excess carrier injection level of $\Delta n \approx 1.3 \times 10^{15}$ cm^{-3}.

The measured J_0 of all the phosphorus diffusions are plotted in Fig. 2 as a function of the surface dopant concentration N_{Ds}. In most cases, for a given N_{Ds}, there are two or more dopant profiles with different sheet resistances R_{sh}. For example, for $N_{Ds} \approx 1.15 \times 10^{20}$ cm^{-3}, the results show that a low sheet resistance ($R_{sh} = 11.5\,\Omega/\square$), deep diffusion gives a lower J_0 than a high sheet resistance ($R_{sh} = 90.9\,\Omega/\square$), shallower diffusion. This is consistent with computer simulations[14] and with the fact that a shallow diffusion (high R_{sh}) makes the n$^+$ region more "transparent,"[15,16] allowing minority carriers to flow toward the surface and recombine there. The details of the dopant profiles are given in the Table II of the Appendix.
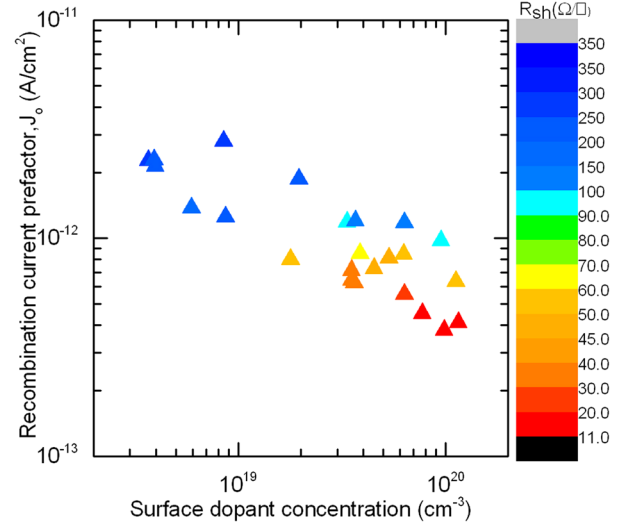
III. COMPARISON BETWEEN MEASURED AND THEORETICAL J_0

In this section we compute theoretically the J_0 corresponding to the measured dopant profiles using Schenk's theoretical BGN model with Fermi-Dirac statistics. To model minority carrier transport and recombination in a non-uniformly doped region we use a simple analytic model,[17] which provides more flexibility than numerical simulations.[18] We have compared the analytic model with the numerical model EDNA[7] by calculating J_0 for several doping profiles, using the same Auger, mobility, and BGN models. The results show that the relative error of the analytical solution is below 0.7%. From its analytical expression,[17] it can be seen that J_0 is sensitive to p_o, τ_p, μ_p, and S_p, the minority carrier concentration, lifetime, mobility, and surface recombination velocity. To determine the product of the electron and hole concentrations in equilibrium $p_0 n_0$, it is necessary to take into account BGN effects.

A. Approaches to determine the $p_0 n_0$ product

At high dopant concentrations, the $p_0 n_0$ product is increased over its normal equilibrium value n_i^2 due to BGN. The effective intrinsic carrier concentration n_{ieff} can be expressed using Fermi-Dirac statistics as

$$p_0 \cdot n_0 = n_{ieff}^2 = n_i^2 \frac{\dfrac{n_o}{N_c}}{\exp\left(F_{1/2}^{-1}\left(\dfrac{n_o}{N_c}\right)\right)} \exp\left(\frac{\Delta E_g}{KT}\right). \quad (1)$$

In this expression ΔE_g represents the "real" BGN. Alternatively, the $p_0 n_0$ product can be expressed by means of an *apparent* BGN ΔE_g^{app} in conjunction with Boltzmann statistics,[19]

$$p_0 \cdot n_0 = n_{ieff}^2 = n_i^2 \exp\left(\frac{\Delta E_g^{app}}{KT}\right), \quad (2)$$

where ΔE_g^{app} is based on electronic measurements by several researchers.[4,19–23]

Fig. 3 shows the $p_0 n_0$ product as a function of the ionized dopant concentration in n-type silicon calculated with Eqs. (1) and (2) using Schenk's BGN[8] and the two BGN expressions derived in Sec. IV. The $p_0 n_0$ product based on Boltzmann statistics increases monotonically as the dopant concentration increases. On the other hand, the Fermi-Dirac approach leads to a maximum of the $p_0 n_0$ product at a dopant concentration of 5×10^{19} cm^{-3} if Schenk's BGN model is used, or 9×10^{19} cm^{-3} in the case of the BGN derived in Sec. IV. This behavior of the $p_0 n_0$ product is due to degeneracy effects, and is a consequence of the properties of the inverse Fermi integral function of order $^1/_2$ in Eq. (1). Above a dopant concentration of 1×10^{18} cm^{-3}, Schenk's BGN model[8] gives significantly lower values for the $p_0 n_0$ product than the other models, which results in an underestimation of the recombination current in n$^+$ regions, as shown below.

B. Simulation results

Simulations of the J_0 of the dopant profiles in this study were performed for a range of possible values of the surface recombination velocity S_p to confirm that, within a relative error of 3%, J_0 remains approximately unchanged for S_p in the range of 3×10^6 cm/s to 1×10^7 cm/s.[4,24] Such 3% uncertainty in J_0 produces an error of less than 1% in extracting the BGN. Thus, it is reasonable to use $S_p = 3 \times 10^6$ cm/s, the same value used in Ref. 4 for metal-coated diffused regions, as representative of the thermal velocity of carriers in silicon.

In the bulk of the heavily doped region, recombination processes are represented by τ_p, the minority carrier lifetime. At high dopant concentrations, where carrier-carrier interactions are stronger, τ_p is dominated by Auger recombination.

There are several empirical Auger recombination models proposed by Dziewior and Schmid,[25] Kerr and Cuevas,[26] Altermatt et al.,[27] Wang and Neugroschel,[28] and Richter et al.[29] In the case of a large S_p, due to the dominance of surface recombination, the different lifetime models produce a maximum relative error of less than 1% on the recombination current pre-factor J_0. In our simulations, we have used the model by Kerr and Cuevas[26] and neglected Shockley Read Hall recombination. Nevertheless, the selection of the lifetime model could have a significant impact in the case of passivated diffused regions.

The effects of minority carrier mobility on the recombination current pre-factor, J_0, have been discussed briefly in Refs. 4 and 30. In "transparent" regions, the flow of minority carriers toward the high recombination region is limited by their diffusivity. As a result, the calculation of J_0 is quite sensitive to which minority mobility model is used. In the simulations shown in this paper, we have used Klaassen's unified mobility model,[31] together with an intrinsic carrier density of $n_i = 9.65 \times 10^9$ cm^{-3} (Ref. 32) at a temperature of 300 K.

For every dopant profile, we have calculated J_0 by applying Eq. (1), to determine the $p_0 n_0$ product. A comparison between the simulated value and the experimental J_0 is presented in Fig. 4. The J_0 measured with a Sinton Instruments photoconductance tester were reevaluated to the same $n_i = 9.65 \times 10^9$ cm^{-3}. In Fig. 4, it is clear that Schenk's BGN model, together with Fermi-Dirac statistics and the above mentioned mobility, cannot reproduce the measurements of J_0 accurately, particularly for diffused regions with a low sheet resistance. Such diffusions have a relatively wide region where the dopant density is very high, making the impact of Fermi-Dirac statistics particularly significant. This leads, as Fig. 3 shows, to a reduced $p_0 n_0$ product and to an underestimation of bulk and surface recombination when Schenk's BGN model is used.
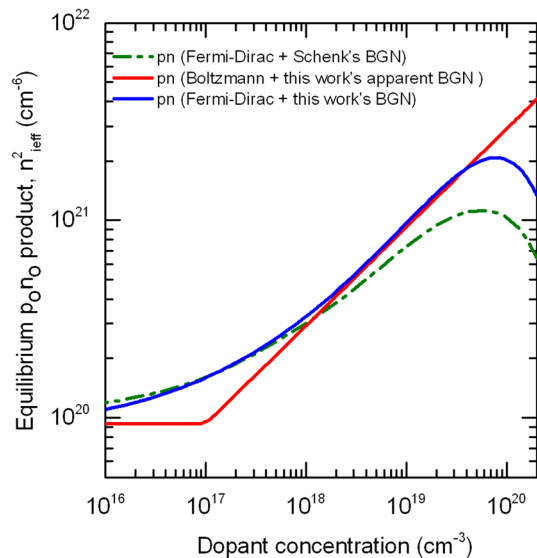

FIG. 3. Calculation of the equilibrium $p_0 n_0$ product in heavily doped n$^+$ silicon as a function of dopant density using the two approaches described in the text. The values obtained with the empirical BGN expressions derived in Sec. IV are compared to those obtained with Schenk's BGN model.[8]
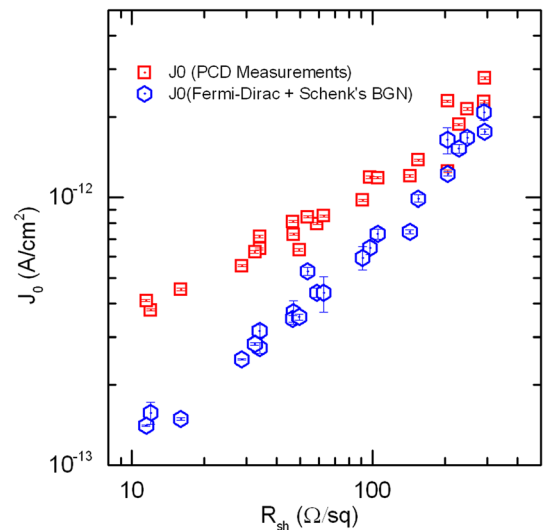

FIG. 4. Measured J_0 as a function of the sheet resistance of the diffusions compared the simulation that based on Fermi-Dirac statistics with Schenk's BGN. The error bars of the simulated values are determined from measurement uncertainties of the dopant profiles.

IV. EXTRACTION OF THE ENERGY BANDGAP NARROWING

From the measurements presented in Sec. II, we have extracted the BGN as a function of dopant density in a manner that is consistent with the measured J_0. As mentioned above, the modeling used to extract the BGN is based on Klaassen's mobility model[31] and $n_i = 9.65 \times 10^9 \, \text{cm}^{-3}$,[32] corresponding to a temperature of 300 K. Schenk's BGN model[8] is quite complex, but we have found that it can be fitted with a simple expression of the form,

$$\Delta E_g^{app}(N_D) = A \left[\ln\left(\frac{N_D}{N_{ref}}\right) \right]^b + C, \qquad (3)$$

where A, b, and C are constants and N_{ref} represents the dopant concentration where BGN effects start to be noticeable. The values for these constants are given in Table I and the accuracy of the approximation is shown in Fig. 5. The coefficient C is only needed to obtain a reasonable approximation for dopant densities below $10^{17} \, \text{cm}^{-3}$.

Based on the same formal dependence of the BGN on dopant density described by Eq. (3), we have analyzed the measured dopant profiles and their corresponding J_0 with Fermi-Dirac statistics using the same exponent b = 3, $N_{ref} = 1 \times 10^{14} \, \text{cm}^{-3}$ and C = 0. Once N_{ref}, b and C have been fixed, it is possible to find the value of the constant A for each dopant profile by an interpolation method, matching the corresponding theoretically simulated J_0 and the measured J_0. Averaging the A values obtained for the different dopant diffusion profiles, given in Table II of the Appendix, we determine $A = 0.042 \, \text{meV}$, with a standard deviation of 0.003 meV, which indicates a low uncertainty in the analysis.

In a similar manner, the measured dopant profiles and J_0 were also analyzed with Boltzmann statistics to obtain an *apparent* BGN model. Based on measured V_{oc} of silicon solar cells as a function of the wafer dopant density[33,34] and previously published *apparent* BGN models,[4,9,15,35] we now use Eq. (3) with b = 1, $N_{ref} = 1 \times 10^{17} \, \text{cm}^{-3}$ and $C = 0 \, \text{meV}$. Following the same interpolation and averaging procedures described above, a coefficient $A = 12.96 \pm 0.7 \, \text{meV}$ is determined. The parameters A and b are almost identical to the previous empirical expression for the *apparent* BGN reported in Ref. 4; the small differences between both are due to the slightly different N_{ref} and mobility values used in Ref. 4.
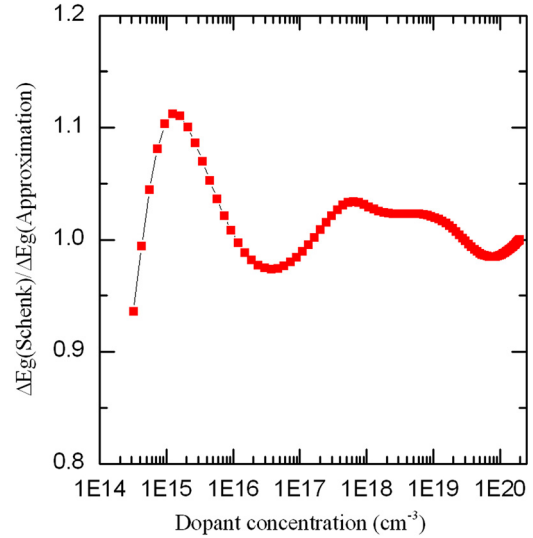

FIG. 5. Ratio between Schenk's BGN at 300 K and its approximation given by Eq. (3) over a broad range of dopant concentrations.

The results of the analysis are summarized in Table I, where the parameters that describe the BGN corresponding to each of the two statistics are given. To check if the two formulations of the BGN derived in this study are consistent with each other, we have plotted in Fig. 3 the respective $p_0 n_0$ products as a function of dopant density. The agreement between both is good over the dopant density range of interest for dopant diffused regions in silicon. Fermi-Dirac statistics give a smaller $p_0 n_0$ product for dopant concentrations above $N_D = 10^{20} \, \text{cm}^{-3}$. Given that the highest dopant density in our experiment is $N_D = 1.15 \times 10^{20} \, \text{cm}^{-3}$, it is not possible to resolve this discrepancy without further work.
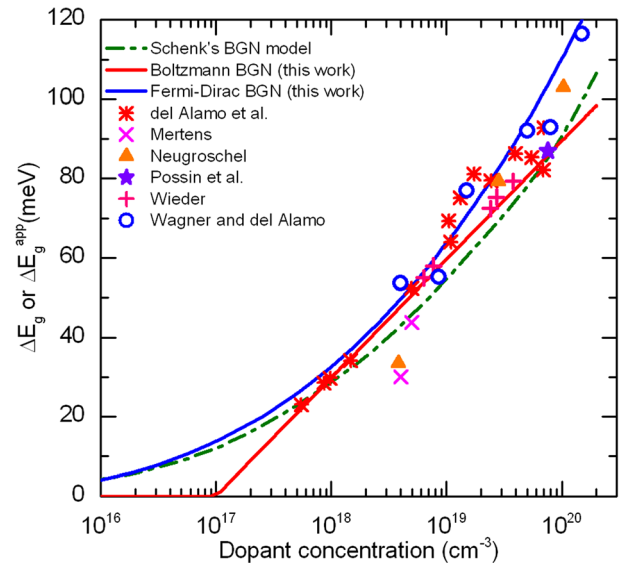
FIG. 6. Energy bandgap narrowing as a function of dopant concentration in n-type silicon. The dashed-dotted line represents Schenk's theoretical model.[8] The continuous lines represent this work's Fermi-Dirac based empirical BGN expression (blue) and the Boltzmann-based *apparent* BGN empirical expression (red). Electronic measurements by del Alamo *et al.*,[19] Mertens and Van,[20] Neugroschel,[21] Possin *et al.*,[22] and Wieder[23] have been corrected with Klaassen's[37] mobility model and $n_i = 9.65 \times 10^9 \, \text{cm}^{-3}$. Photoluminescence measurements from Wagner and Alamo.[36]

TABLE I. Parameters of the two empirical BGN models derived in this work using either Boltzmann or Fermi-Dirac statistics. The previous *apparent* BGN model of Ref. 4, reevaluated for $n_i = 9.65 \times 10^9 \, \text{cm}^{-3}$, and an approximation to Schenk's BGN model are also given.

	A (meV)	N_{ref} (cm^{-3})	b	C (meV)
Previous *apparent* BGN model[4]	13.04	1.4×10^{17}	1	0
Boltzmann based *apparent* BGN (this work)	12.96 ± 0.70	1×10^{17}	1	0
Parameterization of Schenk's BGN	0.035	1×10^{14}	3	0.87
Fermi-Dirac based BGN (this work)	0.042 ± 0.003	1×10^{14}	3	0

The empirical dependence of ΔE_g on dopant density determined with Fermi-Dirac statistics (blue continuous line) and the empirical ΔE_g^{app} determined with Boltzmann statistics (red line) are compared in Fig. 6 to Schenk's BGN model (dashed green line). The experimental values reported in literature[19–23,36] are also shown. Despite the significant scattering in the data, the empirical ΔE_g derived in this paper tends to agree well with photoluminescence[36] measurements of the BGN. On the other hand, the empirical ΔE_g^{app} tends to be in better agreement with electrical measurements of the *apparent* BGN. Visually, the difference between the three models in Fig. 6 is deceptively small, at high dopant densities such difference in BGN leads to a large (more than a factor of two) discrepancy in J_0, as discussed in Sec. III.

V. CONCLUSION

When modeling phosphorus doped regions with Fermi-Dirac statistics, Schenk's theoretical model for the energy band gap narrowing leads to underestimating the recombination current in those regions. To obtain agreement between theory and experiment it is necessary to use a higher BGN, as derived in this paper.

Alternatively, highly doped regions can be modeled with Boltzmann statistics and an *apparent* BGN. Based on a broad range of dopant profiles and J_0 measurements, an empirical expression for the *apparent* BGN has been derived in this paper and found to be in good agreement with a broadly used previous *apparent* BGN model.

The two empirical BGN models, used in conjunction with the appropriate statistics, are equivalent in the context of the diffused regions examined in this work, which feature a very high surface recombination velocity. Such equivalence cannot be stated to be general without further testing, but it can be expected to hold for most phosphorus diffused regions encountered in silicon solar cell technology.

APPENDIX: SUMMARY OF THE PHOSPHORUS DIFFUSED SAMPLES

TABLE II. Summary of the phosphorus diffusions used in this work, including sheet resistance, surface concentration, and approximate diffusion depth. The J_0 measurements of the aluminium coated diffusions are shown, revaluated for $n_i = 9.65 \times 10^9$ cm^{-3}. The corresponding coefficients A calculated in Sec. IV by using either Boltzmann or Fermi-Dirac statistics are also given.

Sample	R_{sh} ($\Omega/\square$)	N_s (cm^{-3})	Diffusion depth (μm)	J_0(measured) (fA/cm^2)	A (Fermi-Dirac Statistics) (meV)	A (Boltzmann Statistics) (meV)
1	11.5 ± 0.4	$1.15 \pm 0.05 \times 10^{20}$	1.33	411	4.54×10^{-2}	13.3
2	12.0 ± 0.4	$9.83 \pm 0.18 \times 10^{19}$	1.53	379	4.36×10^{-2}	12.9
3	16.0 ± 0.9	$7.71 \pm 0.18 \times 10^{19}$	1.46	453	4.63×10^{-2}	13.9
4	28.7 ± 2.6	$6.32 \pm 0.04 \times 10^{19}$	1.13	555	4.50×10^{-2}	13.7
5	32.5 ± 2.7	$3.62 \pm 0.07 \times 10^{19}$	1.02	625	4.34×10^{-2}	13.5
6	34.0 ± 2.7	$3.51 \pm 0.02 \times 10^{19}$	0.98	714	4.37×10^{-2}	13.6
7	40.5 ± 3.7	$3.19 \pm 0.04 \times 10^{19}$	0.83	642	4.42×10^{-2}	13.8
8	46.7 ± 3.8	$5.33 \pm 0.06 \times 10^{19}$	0.77	812	4.36×10^{-2}	13.4
9	47.0 ± 3.9	$4.51 \pm 0.19 \times 10^{19}$	0.85	729	4.34×10^{-2}	13.7
10	49.6 ± 4.3	$1.12 \pm 0.07 \times 10^{20}$	0.71	636	4.18×10^{-2}	12
11	53.8 ± 4.7	$6.26 \pm 0.06 \times 10^{19}$	0.70	847	4.33×10^{-2}	13.4
12	58.8 ± 5.1	$1.79 \pm 0.01 \times 10^{19}$	0.87	799	4.20×10^{-2}	13.2
13	62.7 ± 7.3	$3.87 \pm 0.04 \times 10^{19}$	0.67	853	4.24×10^{-2}	13.1
14	90.9 ± 7.8	$9.47 \pm 0.14 \times 10^{19}$	0.56	973	3.98×10^{-2}	12.1
15	97.6 ± 7.9	$3.34 \pm 0.11 \times 10^{19}$	0.62	1188	4.27×10^{-2}	13.5
16	105.0 ± 8.4	$6.33 \pm 0.06 \times 10^{19}$	0.40	1182	4.01×10^{-2}	12.4
17	143.0 ± 12	$3.66 \pm 0.06 \times 10^{19}$	0.36	1200	3.99×10^{-2}	12.4
18	155.3 ± 13	$5.95 \pm 0.03 \times 10^{18}$	0.73	1376	3.99×10^{-2}	13
19	205.0 ± 17	$3.93 \pm 0.20 \times 10^{18}$	0.47	2287	4.11×10^{-2}	13
20	205.4 ± 16	$8.68 \pm 0.22 \times 10^{18}$	0.65	1250	3.63×10^{-2}	11.4
21	228.6 ± 18	$1.96 \pm 0.38 \times 10^{19}$	0.28	1869	3.67×10^{-2}	12
22	247.6 ± 19	$3.97 \pm 0.03 \times 10^{18}$	0.43	2137	3.92×10^{-2}	12.4
23	291.0 ± 23	$3.67 \pm 0.29 \times 10^{18}$	0.57	2276	3.82×10^{-2}	12
24	292.5 ± 24	$8.51 \pm 0.17 \times 10^{18}$	0.26	2784	4.20×10^{-2}	13.3

[1]R. J. Van Overstraeten and R. P. Mertens, Solid-State Electron. **30**, 1077 (1987).

[2]H. P. D. Lanyon, Sol. Cells **3**, 289 (1981).

[3]M. A. Green, J. Appl. Phys. **67**, 2944 (1990).

[4]A. Cuevas, P. A. Basore, G. Giroult-Matlakowski, and C. Dubois, J. Appl. Phys. **80**, 3370 (1996).

[5]D. A. Clugston and P. A. Basore, in *Conference Record of the Twenty-Sixth IEEE Photovoltaic Specialists Conference* (1997), p. 207.

[6]*Sentaurus Device* User *Guide* Version C-2009.06 (Synopsis, 2009).

[7]K. R. McIntosh and P. P. Altermatt, in *35th IEEE Photovoltaic Specialists Conference (PVSC)* (2010), p. 2188.

[8]A. Schenk, J. Appl. Phys. **84**, 3684 (1998).

[9]R. R. King and R. M. Swanson, IEEE Trans. Electron Devices **38**, 1399 (1991).

[10]M. J. Kerr, J. Schmidt, A. Cuevas, and J. H. Bultman, J. Appl. Phys. **89**, 3821 (2001).

[11]R. Bock, P. P. Altermatt, and J. Schmidt, in *23rd European Photovoltaic Solar Energy Conference and Exhibition, 1–5 September 2008, Valencia, Spain* (WIP-Renwable Energies, Munich, Germany, 2008), p. 1510.

[12]D. E. Kane and R. M. Swanson, in *IEEE Photovoltaic Specialists Conference* 1985.

[13]R. A. Sinton and A. Cuevas, Appl. Phys. Lett. **69**, 2510 (1996).

[14]R. R. King, R. A. Sinton, and R. M. Swanson, IEEE Trans. Electron Devices **37**, 365 (1990).

[15]J. A. del Alamo and R. M. Swanson, IEEE Trans. Electron Devices **31**, 1878 (1984).

[16]A. Cuevas and M. A. Balbuena, IEEE Trans. Electron Devices **36**, 553 (1989).

[17]A. Cuevas, R. Merchan, and J. C. Ramos, IEEE Trans. Electron Devices **40**, 1181 (1993).

[18]A. Kimmerle, A. Wolf, U. Belledin, and D. Biro, Energy Procedia **8**, 275 (2011).

[19]J. A. del Alamo, S. E. Swirhun, and R. M. Swanson, Solid-State Electron. **28**, 47 (1985).

[20]R. P. Mertens, J. L. Van Meerbergen, J. F. Nijs, R. J. Van Overstraeten, IEEE Trans. Electron Devices **27**(5), 949–955 (1980).

[21]A. Neugroschel, P. Shing Chong, and F. A. Lindholm, IEEE Trans. Electron Devices **29**, 894 (1982).

[22]G. E. Possin, M. S. Adler, and B. J. Baliga, IEEE Trans. Electron Devices **31**, 3 (1984).

[23]A. W. Wieder, IEEE J. Solid-State Circuits **15**, 467 (1980).

[24]P. P. Altermatt, J. O. Schumacher, A. Cuevas, M. J. Kerr, S. W. Glunz, R. R. King, G. Heiser, and A. Schenk, J. Appl. Phys. **92**, 3187 (2002).

[25]J. Dziewior and J. Schmid, Appl. Phys. Lett. **31**, 346 (1977).

[26]M. J. Kerr and A. Cuevas, J. Appl. Phys. **91**, 2473 (2002).

[27]P. P. Altermatt, J. Schmidt, G. Heiser, and A. G. Aberle, J. Appl. Phys. **82**, 4938 (1997).

[28]C. H. Wang, K. Misiakos, and A. Neugroschel, IEEE Trans. Electron Devices **37**, 1314 (1990).

[29]A. Richter, S. W. Glunz, F. Werner, J. Schmidt, and A. Cuevas, Phy. Rev. B **86**, 165202 (2012).

[30]J. A. del Alamo and R. M. Swanson, Jpn. J. Appl. Phys. **26**, 1860 (1987).

[31]D. B. M. Klaassen, Solid-State Electron. **35**, 953 (1992).

[32]K. Misiakos and D. Tsamakis, J. Appl. Phys. **74**, 3293 (1993).

[33]P. Altermatt, J. Comput. Electron. **10**, 314 (2011).

[34]S. W. Glunz, J. Dicker, and P. P. Altermatt, in *Proceedings of the 17th EU Photovoltatic Energy Conference* (WIP-Renewable Energies, Munich, Germany, 2001), p. 1391.

[35]J. del Alamo, S. Swirhun, and R. M. Swanson, Solid-State Electronics **28**, 47–54 (1985).

[36]J. Wagner and J. A. del Alamo, J. Appl. Phys. **63**, 425 (1988).

[37]D. B. M. Klaassen, J. W. Slotboom, and H. C. de Graaff, Solid-State Electron. **35**, 125 (1992).